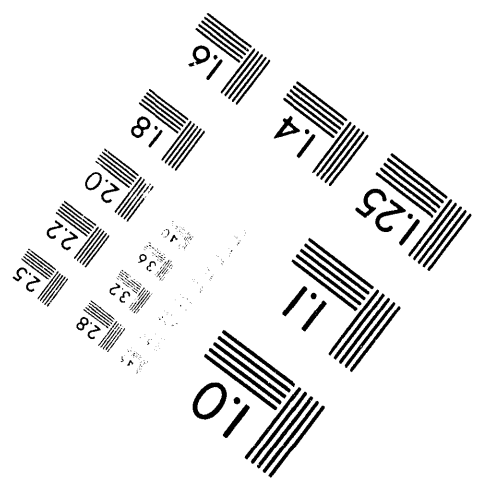
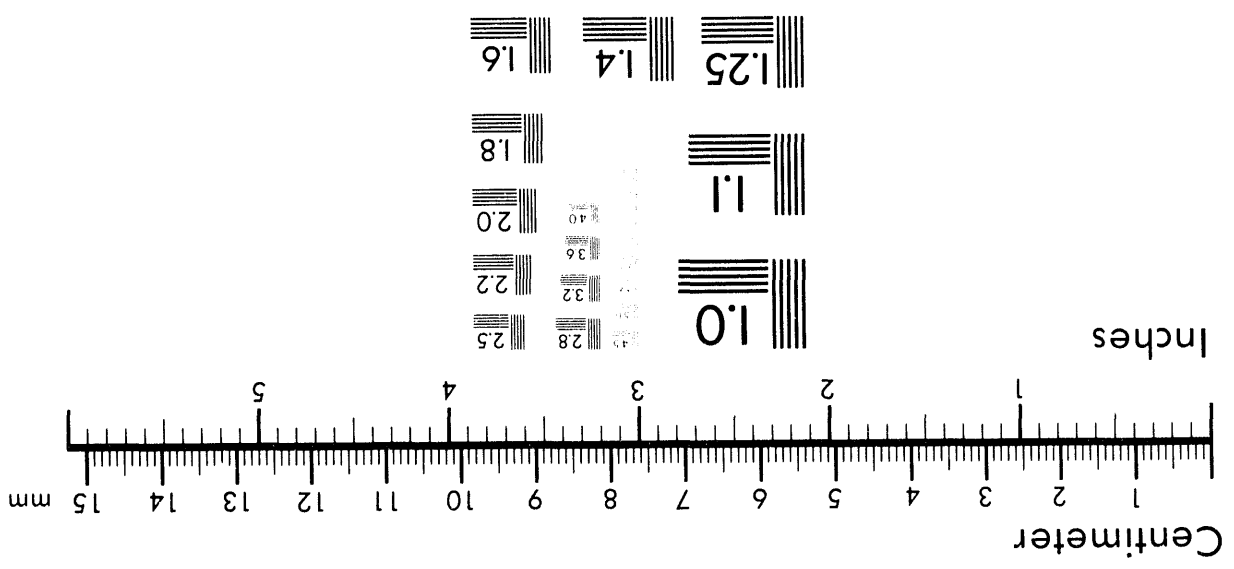
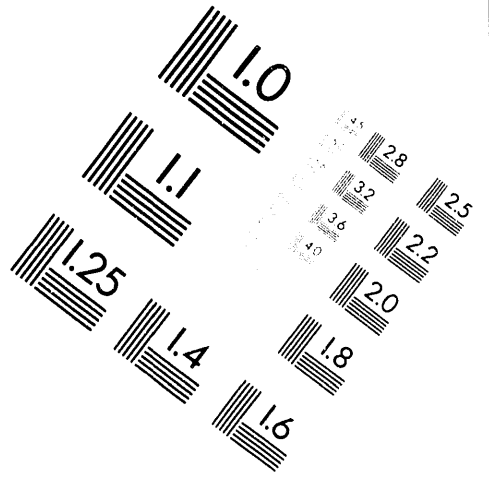
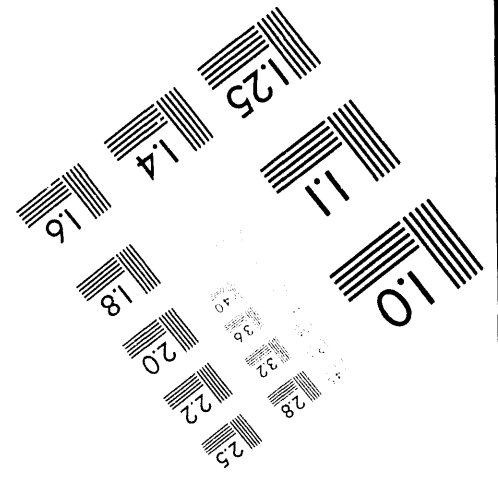


MANUFACTURED TO AIM STANDARDS
 BY APPLIED IMAGE, INC.



Association for Information and Image Management
 1100 Wayne Avenue, Suite 1100
 Silver Spring, Maryland 20910
 301/587-8202



1 of 1

**Sodium laser guide star system at Lawrence Livermore National Laboratory:
system description and experimental results**

Kenneth Avicola, James Brase, James Morris, Horst Bissinger, Herbert Friedman,
Donald Gavel, Rodney Kiefer, Claire Max, Scot Olivier, David Rapp, Thad Salmon
David Smauley, and Kenneth Waltjen

Lawrence Livermore National Laboratory
P.O. Box 808, L-471, Livermore, CA 94550

ABSTRACT

The architecture and major system components of the sodium-layer laser guide star system at LLNL will be described, and experimental results reported. The subsystems include the laser system, the beam delivery system including a pulse stretcher and beam pointing control, the beam director, and the telescope with its adaptive-optics package. Details of the adaptive-optics package and experimental results related to wavefront detection and closed-loop correction will be presented in a companion paper in this conference¹.

The laser system is one developed for the Atomic Vapor Laser Isotope Separation (AVLIS) Program. This laser system can be configured in various ways in support of the AVLIS program objectives, and was made available to the guide star program at intermittent times on a non-interference basis. The first light transmitted into the sky was in July of 1992, at a power level of 1.1 kW. The laser pulse width is about 32 ns, and the pulse repetition rate was 26 kHz for the 1.1 kW configuration and 13 kHz for a 400 W configuration. The laser linewidth is tailored to match the sodium D₂ absorption line, and the laser system has active control of beam pointing and wavefront quality.

Because of the short pulse length the sodium transition is saturated and the laser power is not efficiently utilized. For this reason a pulse stretcher was developed, and the results of this effort will be reported. The beam is delivered via an evacuated pipe from the laser building to the guide star site, a distance of about 100 meters, and then launched vertically. A beam director provides the means to track the sky in the full AO system, but was not used in the experiments reported here. The return signal is collected by a 1/2 meter telescope with the AO package. This telescope is located 5 meters from the laser launch tube. In addition to the fully instrumented package, smaller packages for photometry, wavefront measurement, and spot image and motion analysis have been used. Although the unavailability of the AVLIS laser precluded a full AO system demonstration, data supporting feasibility and providing input to the system design for a Lick Observatory AO system was obtained.

1. INTRODUCTION

The concept of utilizing the mesospheric sodium-layer at an altitude of about 90 km, excited with a resonantly tuned laser as a means of forming a point reference, or guide star, has been under investigation for several years²⁻⁶. The laser guide star program at LLNL started in 1990 and is a Laboratory funded research and development program. The goal of the initial three year phase, which ended in September of 1993, was to demonstrate the feasibility of closed-loop adaptive optics with sodium laser guide stars. A high average power tunable dye laser system then in routine operation at LLNL provided the laser source for these experiments. This laser system was developed for the Department of Energy's Atomic Vapor Laser Isotope Separation (AVLIS) program⁷, and could easily be tuned to the required 589 nm wavelength and the spectral width broadened to 3 GHz. Sponsorship of the AVLIS program transferred from the DOE to the United States Enrichment Corporation (USEC) in the summer of 1993. Congress established the USEC as a government corporation to manage the enrichment enterprises of the country, with the ultimate goal of privatization. Part of the charter includes decisions on advanced research and development technologies such as AVLIS.

The AVLIS laser system has high beam quality and the average power of about 1 kW is sufficient to provide a usable return signal to the wavefront sensor even with the relatively poor seeing, and resulting small subapertures, at the Livermore site, and the use of a wavefront sensor camera that is less sensitive than the current state-of-the-art. So although the laser power is much greater than the few tens of watts, at most, needed for the astronomical application, it was very useful in these initial feasibility experiments. In order to take full advantage of the laser power, however, a pulse stretcher was required

MASTER

REPRODUCTION OF THIS DOCUMENT IS UNLIMITED

to avoid saturation of the sodium layer. The beam was first launched into the sky in July of 1992, and produced a magnitude 5.1 star. The initial experimental program examined the guide star return signal level, spot size, and spot motion⁸. In addition, the Rayleigh scattering signal return was examined and a wavefront sensor was used to obtain wavefront information from the laser guide star. In parallel with these experiments the pulse stretcher was developed, a beam director was procured and installed, and an adaptive optics package was developed for a 1/2 meter telescope at the site. A complete closed-loop demonstration of atmospheric turbulence correction using the laser guide star was scheduled for the fall of 1993. This was not accomplished because FY94 funding for the AVLIS program, which starts in October, was cut severely and laser operations at high power were terminated. A decision on whether to continue with AVLIS development is expected from the USEC in April of 1994. While the goal of a full adaptive optics demonstration using a laser guide star was not accomplished the results of the experimental program did demonstrate feasibility and the second three year phase, described below, moved ahead.

The goal of the present three year program is to attain, at the end of this period, a full-fledged astrophysical observation program on the Lick Observatory 120 inch Shane telescope using adaptive optics and a laser guide star. In preparation for this, a program of monthly measurements of the seeing conditions at this site was undertaken, starting in early 1993. An adaptive optics package for the Lick 40 inch telescope was designed and installed and the first partially corrected images were obtained in November of 1993^{9,10}. The remaining tasks for FY94 are to install the AO package on the 120 inch telescope for operation with natural guide stars and optimized for observation in the near infrared, and development and installation of a 20 W class laser with its associated beam transport and control systems¹¹. Computer simulations will also be performed to predict results and aid in the analysis of results. In FY 95 the laser will become operational and the astrophysical observations using a laser guide star will start. The present 69 actuator deformable mirror will be replaced with a 127 actuator mirror resulting in improved performance at wavelengths of about 1 micron.

2. LASER AND BEAM TRANSPORT SYSTEM

The AVLIS laser is housed in a large building at a distance of about 100 m from the laser guide star site. A schematic diagram of a single dye chain is shown in Figure 1. The nominal output power from a single dye chain, as used in the laser guide star experiments, is 1.3 kW. The power actually launched, at the end of the beam transport system was about 1.1 kW. The pulse repetition frequency is up to 26 kHz in multiples of 4.4 kHz and the pulse width is about 32 ns FWHM. Wavefront quality is typically better than $\lambda/10$ and center optical frequency stability is ± 50 MHz. For the guide star application the center wavelength is 589 nm and the spectral width was tailored to two lines about 1 GHz wide separated by 1.7 GHz. The high beam quality is achieved and maintained by means of a deformable mirror, and a pointing jitter of less than 5 μ rad is obtained with the use of a high bandwidth closed-loop control system.

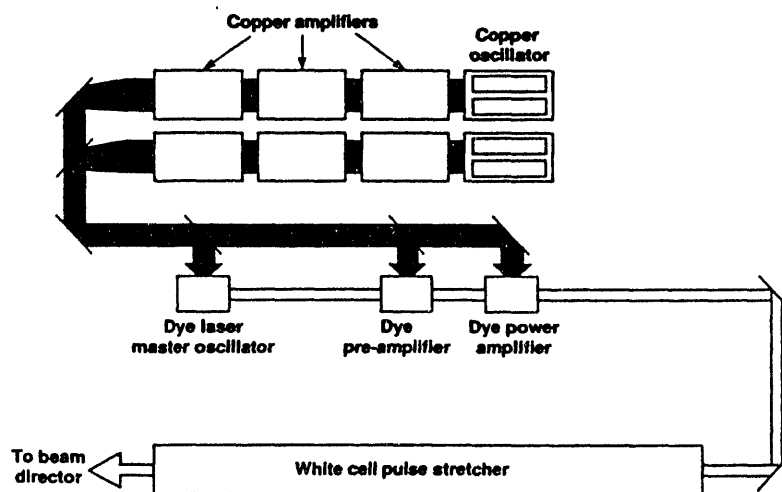


Figure 1. Schematic diagram of a dye laser amplifier chain

For the laser operating at 1 kW with a 32 ns pulse width and a 26 kHz repetition rate, the irradiance at the sodium layer is about 75 W/cm^2 for a one meter spot diameter. This is about 15 times greater than the sodium D₂ resonance line saturation level. If the pulse width is stretched the peak power is reduced with a resulting increase of the return signal level. To realize this process efficiency increase, a pulse stretcher was designed and installed. A schematic diagram illustrating the operation of the pulse stretcher is shown in Figure 2. The 50/50 splitter directs half the input pulse into a delay cell which delays the pulse by one pulse width. The delayed and original pulses are combined and half the pair is delayed by two times the original pulse width. This process is repeated until sixteen pulses have been generated and stacked end to end. The two output beams can be launched side by side or combined into a single beam with a polarizer as shown. A White cell arrangement was used for the delay cells, and the result of testing with a krypton pilot beam is shown in Figure 3. Configurations for both a 16X and a 8X stretch were tested. Testing at high power started in the summer of 1993, and the measured transmission through the stretcher was 80% for the 16X configuration. When first tested in the sky, the observed spot size was about 24 arcsec. Improvements to the alignment of the individual cells reduced the spot size to about 11 arcsec and it was determined that much of the remaining excess spot size was due to thermally induced wavefront errors in some of the optics. It was at this point that the AVLIS program funding was cut and the laser shut down. The experiments and results discussed in this paper were performed with no pulse stretcher.

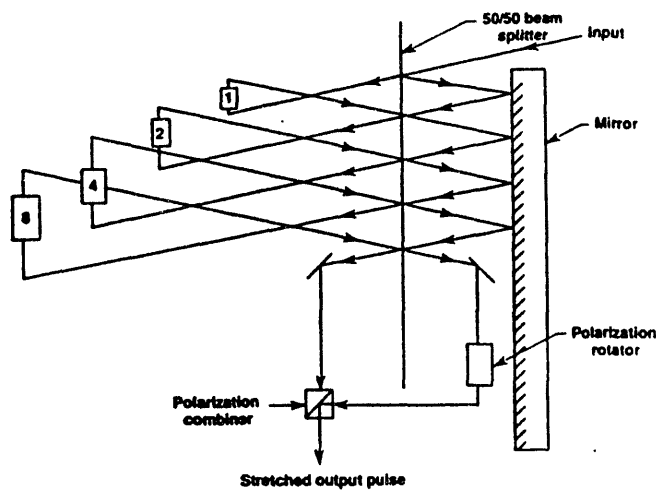


Figure 2. Pulse stretcher with delays of 1,2,4, and 8 times the input pulse width to provide a factor of 16 stretch

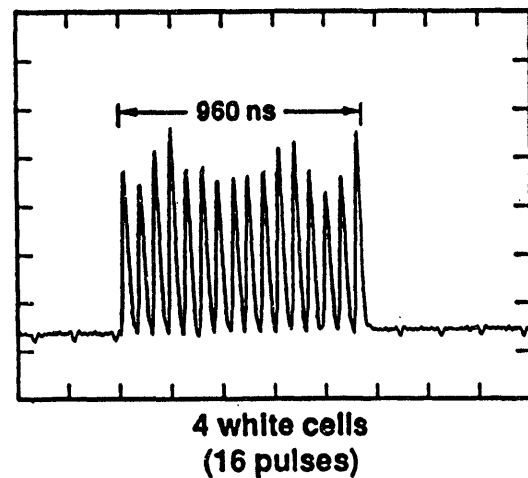


Figure 3. Temporal output of pulse stretcher in which a 24 ns input pulse is stretched to 960 ns.

The beam from the laser building is transported in an underground evacuated pipe to the laser guide star launch site. A photo of the site with the laser operating at 1100 watts is shown in Figure 4. The launch tube is seen in the background, with the 1/2 meter telescope in the right foreground and the 1/4 meter telescope in the left foreground. Near the top of the launch tube is a radar unit linked to a fast shutter which, along with a wide area surveillance radar and visual observer comprise the laser safety system. This photo was taken before the beam director was installed at the top of the launch tube. A beam director was procured in preparation for testing, with a laser guide star, of the adaptive optics package designed for the 1/2 meter telescope. This beam director was designed and fabricated by DFM Engineering. A photo of the unit mounted on top of the launch tube is shown in Figure 5, and the key specifications are listed below.



Figure 4. Photograph of the laser guide star site at Livermore with laser launched into the night sky with a power of 1100 watts.

Laser Beam Director Specifications

Beam director system type	2 mirror system, alt-az mount
Operating range capability	Horizon to zenith in elevation, $\pm 180^\circ$ azimuth
Limit switch setting	35° from zenith in elevation, $\pm 180^\circ$ in azimuth
Instrument package area and capacity	0.25 x 0.5 meters, 50 lb.
Pointing accuracy	< 20 arc seconds rms within 35° of zenith
Relative pointing accuracy	< 3 arc seconds rms open loop for moves $< 5^\circ$
Sidereal tracking	< 2 arc seconds rms open loop for 10 minutes
Zenith tracking exclusion angle	$< 1^\circ$

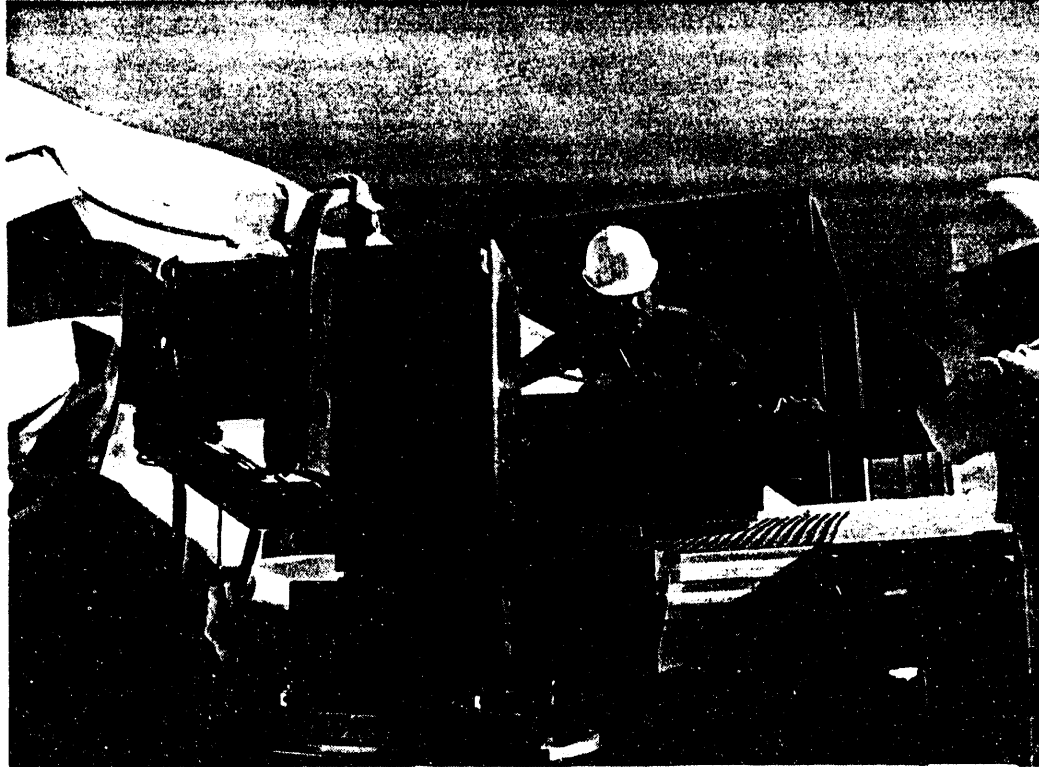


Figure 5. Photograph of beam director mounted on laser beam launch tube.

3. TELESCOPES AND INSTRUMENTATION

The telescopes used in the experiments were offset from the laser by 5 meters, as shown in figure 6. For all the experiments reported here the laser was pointed to zenith. The beam cross section at launch is 4 x 8 cm, and the long axis is aligned to the line joining the laser and telescope position. Diffraction being less in the long dimension compensates for the image elongation that occurs in this axis due to the viewing angle and the thickness of the sodium layer, which is about 10 km. The result is a spot which is roughly circular.

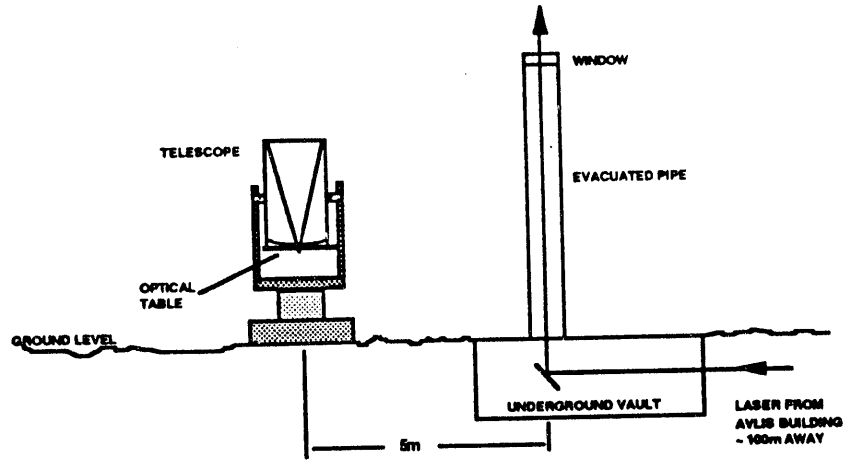


Figure 6. Layout of laser guide star experimental site.

The two telescopes used in these experiments are a 1/2 meter Ritchey-Chretien Cassegrain, and a 1/4 meter Schmidt Cassegrain. For the photometry experiments a Photometrics series 200 camera with a Kodak 1035 x 1320 pixel CCD was used. The pixel size is 6.8 μ m for this CCD. This instrument was used to make photometric measurements using both telescopes. The general arrangement for the photometry experiments is shown in Figure 7. The plate scale was 0.44 arc seconds/pixel on the 1/4 meter and 1.0 arc seconds/pixel on the 1/2 meter telescope. A Kodak EktaPro model 1012 fast framing camera on the 1/2 meter telescope was used for both motion analysis of the laser guide star and for wavefront measurements. This camera uses a two stage intensifier and can frame at up to 1000 frames/second in the full frame mode. A Hartmann wavefront sensor is formed with the use of a Corning lenslet array. The lenslet array had a center-to-center spacing of 524 μ m and a clear aperture for each lenslet of 474 μ m. The optical system magnification of 160 results in each subaperture of the wavefront sensor having a clear aperture of 7.6 cm referred to the telescope primary. The layout for the wavefront sensor experiments is shown in Figure 8. More information on the Kodak camera and its sensitivity when used in the wavefront sensor application can be found in reference 12, and additional details on the hardware and experimental configurations used in these experiments can be found in reference 8. A broader overview of these experiments as well as the implications to adaptive optics for astronomy is given in reference 13.

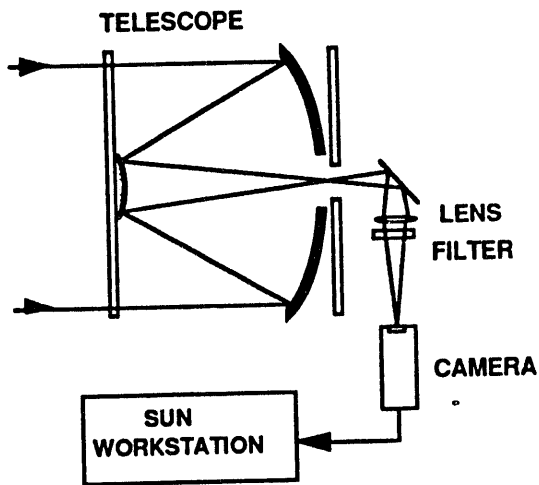


Figure 7. Schematic of hardware used in imaging and motion analysis experiments.

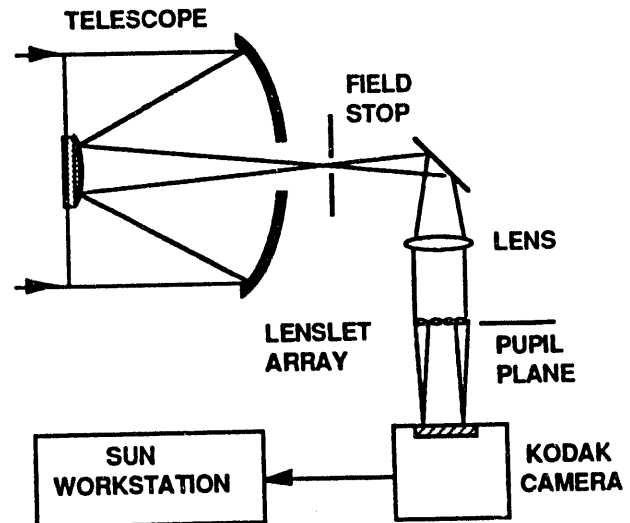


Figure 8. Schematic of wavefront sensing optical arrangement.

A complete adaptive optics package for the 1/2 meter telescope was designed, fabricated and assembled. This work is described in reference 1, also in this proceeding. Part of this AO package is a tip-tilt system which was tested independently and will be described here. The sensor for this system is a quadrant silicon avalanche photodiode (APD). The active mirror is a Polytec PI model S-330 tilt stage and the controller was designed and fabricated at LLNL. A schematic diagram of the tip-tilt system is shown in Figure 8, and Figure 9 is a photograph of the major components.

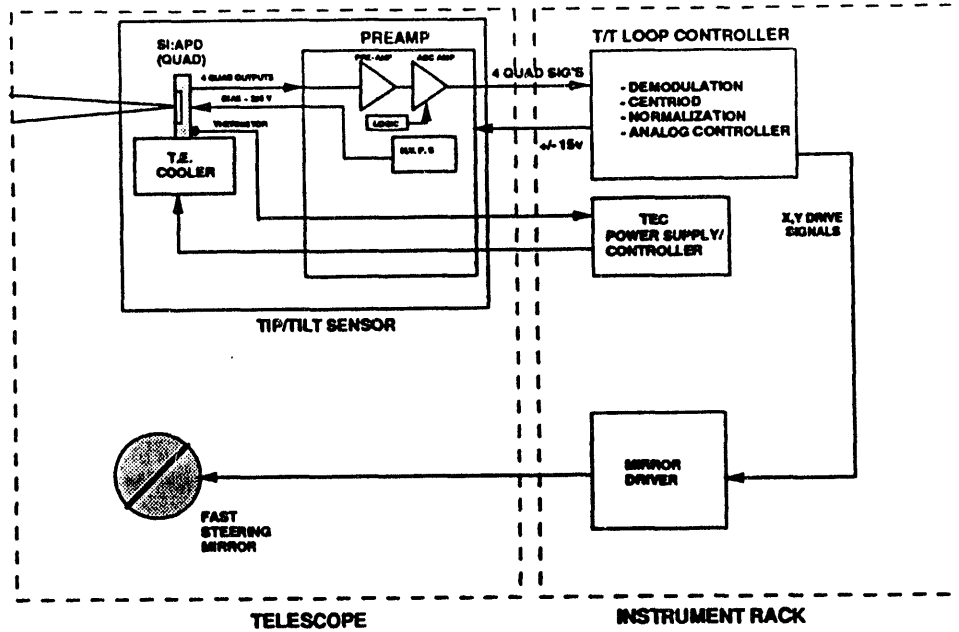


Figure 8. Schematic diagram of the tip-tilt system

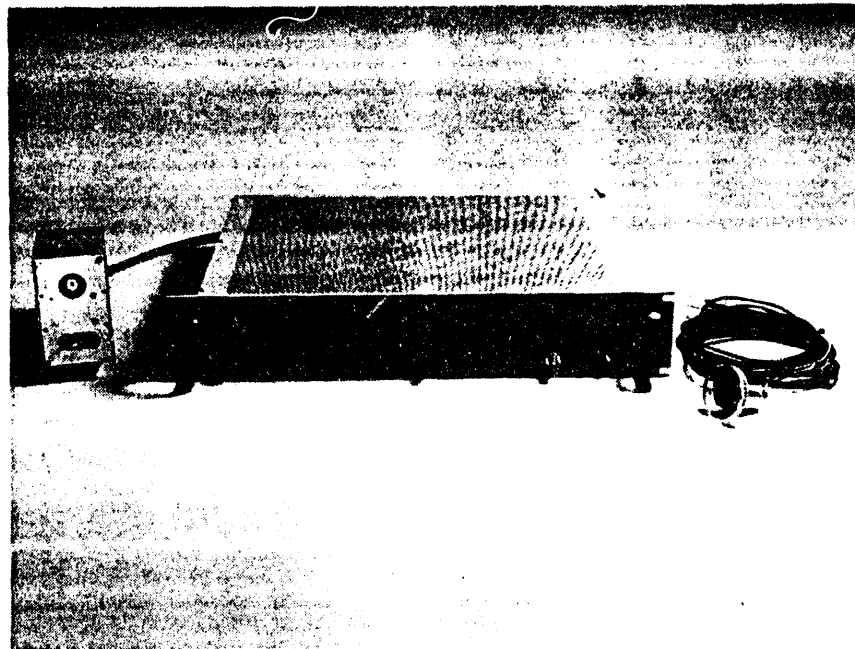


Figure 9. Photograph of the tip-tilt system components: sensor head, controller, and tilt stage.

The analog controller for the tip-tilt system was designed to provide a selectable bandwidth so that, depending on seeing conditions, the optimum bandwidth can be used. When the atmospheric disturbance spectrum is predominantly of low frequency, a low loop bandwidth can be used. In this case S/N is maximized permitting operation with higher magnitude (dimmer) reference stars. When the disturbance frequencies are high, the higher loop bandwidths must be used to obtain the disturbance rejection needed. The selectable bandwidths are 30, 60, and 120 Hz. The bandwidth as used here refers to the closed loop gain crossover frequency, the frequency at which there is no disturbance rejection. The closed loop disturbance rejection performance of the system, as measured in the laboratory, is shown in figure 10. The silicon avalanche quadrant APD used in the system described here is the EG&G model C30927E. A more sensitive tip-tilt sensor based on four EG&G model SPCM-200-PQ photon counting detectors and a quadrant fiber array is presently under development.

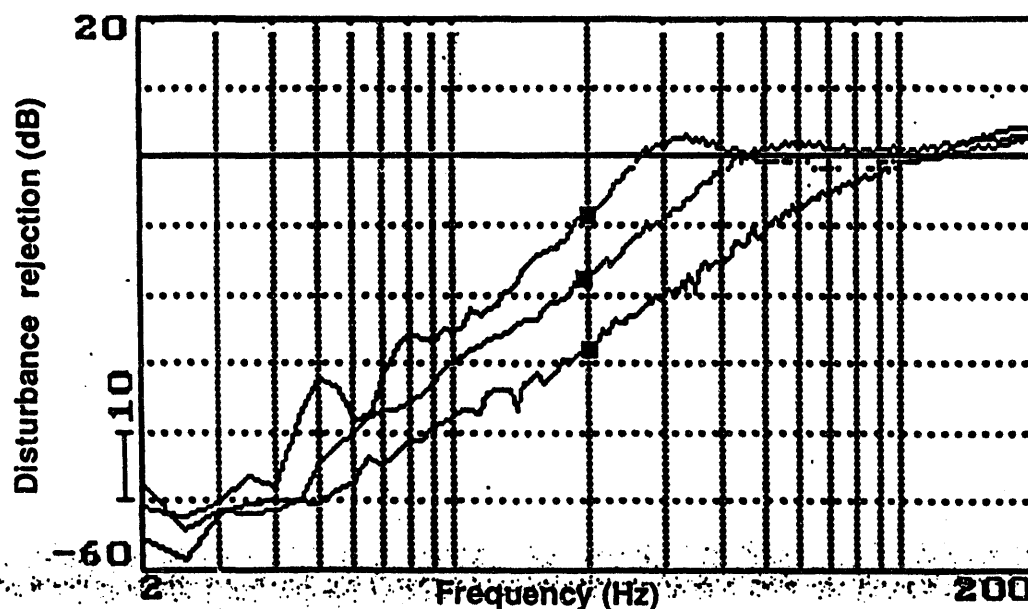


Figure 10. Closed loop disturbance rejection performance of the tip-tilt system for the three selectable bandwidths.

4. EXPERIMENTAL RESULTS

4.1 Laser guide star size and motion

The Photometrics camera was used on the 1/4 meter telescope to observe the laser guide star image and to perform the photometric measurements reported in the next section. The series of photographic images in Figure 11 are the images obtained for laser power ranging from 1100 watts to 7 watts. Longer exposure times were required as the laser power decreased, as indicated in this figure. The Rayleigh backscatter in the lower atmosphere as well as the return from the sodium layer at an altitude of about 90 km can be seen in these images. The average guide star spot size with the laser power at 1100 watts was 7 arc seconds FWHM, in the 3 second exposure. This is the emission spot size, and because the sodium transition is saturated at this power level the wings in the beam produce a higher return signal compared to the spot center than would be the case if the irradiance were below saturation. The 7 arcsec angular size correspond to a FWHM spot diameter of 3.0 meters at the sodium layer. Taking account of the saturation effect on the emission spot size, the incident irradiance spot size was about 2.0 meters. The diffraction limited angular size, using the 4 cm beam dimension, is $\lambda/d = 14.1$ r. This corresponds to a spot diameter of 1.4 m FWHM. The expected reduction in emission spot size as the laser power was reduced was not

observed in this experiment. Possible causes for this include changes in beam quality or pointing jitter as the laser power was reduced. The most likely cause is increasing pointing jitter since the high bandwidth pointing control loops for the AVLIS laser were designed to operate at the higher laser powers and do not control at the lower levels used in these experiments. The long exposures, 48 seconds at the 7 watt power level, result in image enlargement in the presence of pointing jitter. In a later experiment in which the laser power was reduced by another method, which maintained active beam control, the observed spot diameter was 5 arcsec FWHM with a laser power of 8 watts. This is about 1.7 times the diffraction limit for the 4 cm aperture.

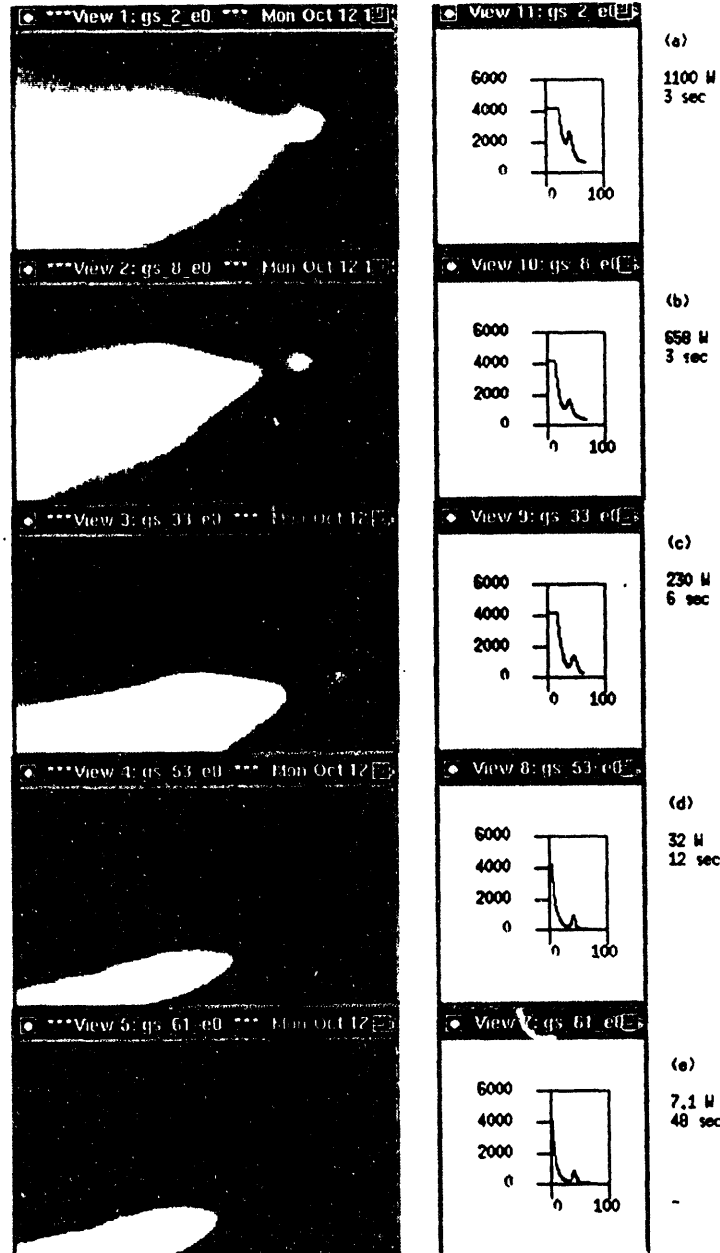


Figure 11. Laser guide star images produced with laser power ranging from 1100 to 7 watts, and exposure times as indicated.

The motion of the laser guide star spot at the 1100 watt power level was measured using the Kodak fast framing camera on the 1/2 m telescope. 100 frames were taken at a frame rate of 125 frames/second. For each frame the spot centroid was calculated, providing a time record of 0.8 seconds of the x and y axis motion. The 2-axis rms motion for a natural star the laser guide star, and laser guide star with the high bandwidth pointing control off, were 0.60, 0.66, and 0.90 arc seconds respectively. The observed motion of the natural star is due to the atmosphere and any telescope motion. The motion of the laser guide star is due to laser pointing jitter, telescope motion, and the atmospheric effects. The measured motions are somewhat under estimated since the 0.8 second time record does not include frequencies below about 1.2 Hz.

4.2 Photometry

The irradiance at the ground from the laser guide star was measured using the calibrated Photometrics camera. Experiments were performed with this camera on both the 1/4 m and 1/2 m telescopes. The irradiance at the telescope input is given by $H_g = (S_g R_\lambda) / (A_t T_t I)$,

where S_g is the camera total output signal in the star image in digital or data numbers (DN), R_λ is the camera response at 589 nm (photons/DN), A_t is the telescope collection area, T_t is the telescope transmission at 589 nm, and I is the integration time. The atmospheric transmission at 589 nm could also be determined with the aid of standard stars, which are stars for which the spectral irradiance above the atmosphere has been measured.

To eliminate any contribution from the Rayleigh backscatter in the laser guide star image, and also to subtract sky background, a method involving detuning of the laser off the sodium absorption line was used. Two frame were taken in rapid succession, the first with the laser tuned to the 589 line and modulated to match the line width, and the second with the laser tuned off by 2.6 GHz and not modulated. To arrive at the signal photons from just the sodium return, the images were processed by counting just the DN pixel values in a 16 arcsec circle centered on the guide star. The DN values from the same pixel area of the image with the laser detuned was then subtracted. The irradiance from the guide star obtained in this manner is shown in Figure 12, and compared with simulation model predictions. The simulation used a 24-level density matrix calculation to predict the backscatter emission rate¹⁴ as a function of pulse fluence at the sodium layer. The calculations used laser parameters matching those of the experimental laser and assumed an irradiance spot size of 2 meters. A sodium column density of $4.1 \times 10^9 \text{ cm}^{-2}$, which is a least squares fit to the experimental measurements at the five laser power levels, was used.

The data of Figure 12 was taken on the night of August 27, 1992 with the 1/4 m telescope, and the atmospheric transmission was 60%. This same data is shown in Figure 13 along with data taken on the 1/2 m telescope on the nights of October 6 and 7, 1992, for which the atmospheric transmission was about 53% and 47% respectively. Variations in the sodium column density, in addition to the changes in atmospheric transmission, account for the variation in return signal irradiance. The saturation effect at the higher power levels is clearly seen.

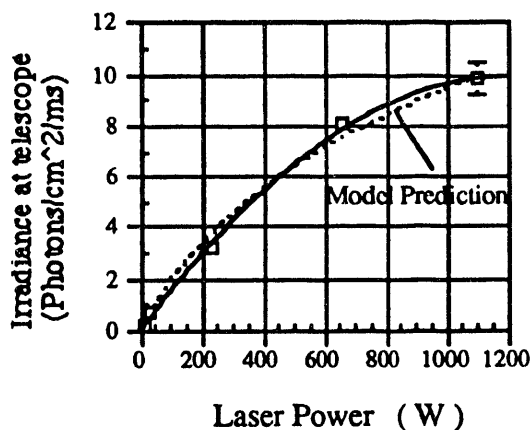


Figure 12. Sodium backscatter irradiance at the ground as function of laser power; experiment results and model predictions.

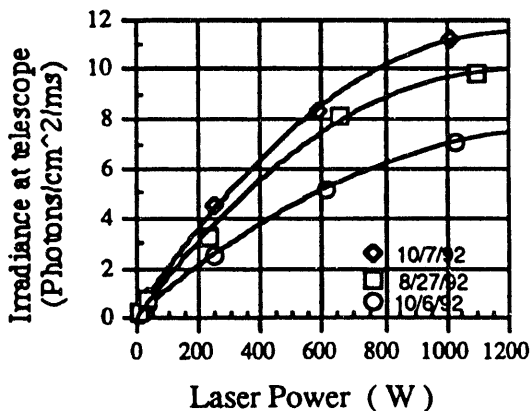


Figure 13. Sodium backscatter irradiance at the ground on August 27, and October 6 and 7, 1992.

4.3 Wavefront reconstruction from laser guide star reference

The optical arrangement illustrated in Figure 8 was used to acquire wavefront information using the laser guide star as the point reference. The Kodak fast framing camera on the 1/2 m telescope was used in a Hartmann wavefront sensor configuration, as described in section 3. The 6 x 6 array of Hartmann subapertures, with a spacing of 8.4 cm, forms an array of spots on the camera. A laser power of 875 watts was used, and the guide star return signal was sufficient to frame the camera at 125 frames/second with an exposure time of 5 ms. The Hartmann sensor converts incoming wavefront slope changes into spot centroid changes. From this information the wavefront phase can be reconstructed. The power spectra of the subaperture tilts can be obtained by averaging the Fourier transforms of the tilts of all the Hartmann subapertures. Data was also taken with a natural star (Capella). Because this star is brighter the camera was framed at 1000 Hz with 1 ms exposures. Figure 14 shows the tilt power spectra for both the laser guide and natural star as the point reference. The spectra for the laser guide star extends to only 62 Hz because of the 125 Hz sample rate, while the spectra for Capella goes out to 500 Hz. At low frequencies both power spectra show the $v^{-2/3}$ scaling predicted for Kolmogorov turbulence. The laser guide star's lower signal-to-noise ratio and larger spot result in a spectra which is a little noisier. The two sets of data were not taken simultaneously, and therefore these are two realizations of the turbulence spectra. However, the average conditions were quite similar as indicated in the figure. The break at about 20 Hz is believed to result from the finite subaperture size and occurs at a frequency corresponding to the wind velocity divided by the subaperture diameter. The slope at higher frequency, which can be seen in the natural star data, is near $v^{-8/3}$ as reported by others.

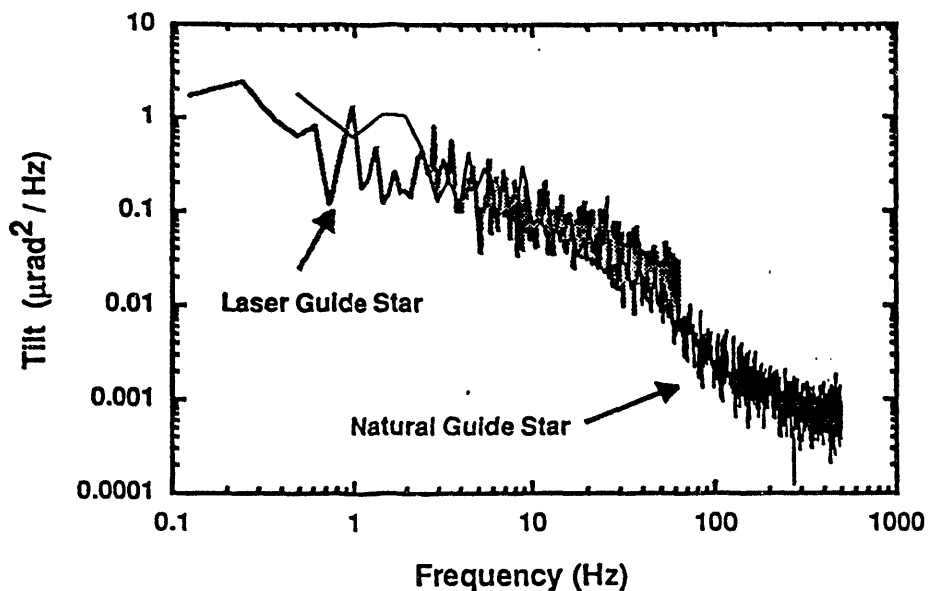


Figure 14. Tilt power spectra using laser guide star and natural star point references, obtained from Hartmann wavefront sensor data.

The wavefront slope data with the laser guide star discussed above was used to reconstruct the wavefront phase. This is a significant step in demonstrating the feasibility of adaptive optics using sodium laser guide stars. Reconstructed wavefronts from three consecutive frames obtained from a laser guide star and a natural star are compared in Figure 15, both sampled at 8 ms intervals. The top row is from the natural star and the bottom row from the laser guide star. The data were taken under similar conditions but not simultaneously. The reconstructions in Figure 15 represent only higher order wavefront errors since the average wavefront tilt was removed from the slope data by subtracting the average centroid positions. The original graphical presentation of this data was in color, and much is lost in the black and white copy of Figure 15. While the details of the reconstructed wavefronts are of course different, since they were not simultaneous, they are qualitatively similar in scale of the distortions. The rms phase fluctuation over the entire data set was 0.52 microns for the laser guide star, and 0.35 for the natural star. The higher value for the laser guide star is partially due to the lower signal-to-noise ratio with this reference. The natural star magnitude, $m_V = 0.1$, is about 100 times brighter than the laser guide star with magnitude of about $m_V = 5$.

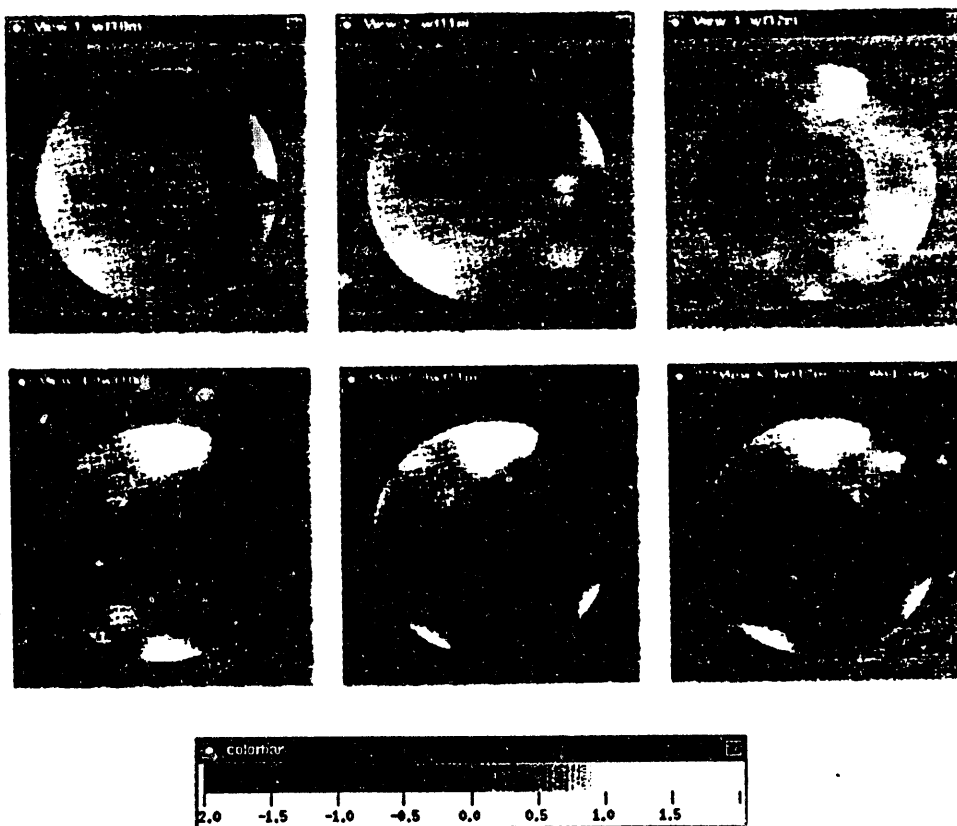


Figure 15. Reconstructed wavefronts from the laser guide star as reference (bottom) and natural reference star (top).

4.4 Rayleigh backscattering

To help understand the physical factors that determine how much Rayleigh scattered light contaminates the laser guide star, we have developed a computational model of the Rayleigh backscatter as imaged by a camera focused on a natural star at the same angular position as the laser guide star. In this model, the atmosphere around the near-vertical laser beam propagation path between 9.5 and 90.5 km altitude is divided into 1 km horizontal layers. The laser beam irradiance at each layer is assumed to be the far-field irradiance profile corresponding to the profile at the laser beam director with its size directly proportional to the layer altitude and with its center shifted to account for the location of the beam axis as seen by the camera. An optical transfer function (OTF) that is the product of telescope and atmospheric OTF's is used to compute the contribution of each layer to the image. The telescope OTF is that of a 0.25 m diameter circular aperture with a defocus quadratic phase; it is computed digitally from the pupil function by fast Fourier transforms. The atmospheric OTF, $\exp[-3.44(\lambda f/r_0)^{5/3}]$, is the long-exposure turbulence OTF¹⁵ for a coherence diameter $r_0 = 5$ cm at 589 nm wavelength, where f is a normalized spatial frequency ($2f$ is the conjugate variable to angular position in radians). The scattering cross section at each layer is proportional to the atmospheric density which is approximated as an exponential with a 7.3 km scale height and a magnitude matched to the 1976 U. S. Standard Atmosphere at sea level.

The effect of a hard-apertured laser beam irradiance profile on the contribution of Rayleigh scattering to the image irradiance along the direction of the projection of the laser beam on the image plane is shown in Figure 16. In the three calculations the laser beam director is 5 m from the observing telescope. The initial beam sizes are chosen to give a 2 m spot diameter at 92 km in the sodium layer (to match our experiments); for the untruncated gaussian (solid line) the full-width at half maximum (FWHM) is used, for the other profiles $\lambda z/w$ is used, where w is the FWHM at the beam director; the numerical values are for a 1 kW laser in the absence of any transmission losses. The untruncated gaussian (solid line) and truncated square-base pyramid prismoid (dotted line) irradiance profiles produce nearly identical images. The hard-apertured uniformly illuminated square irradiance profile (dashed line) generates a 20-fold larger image irradiance at the position of the sodium layer guide star (zero angle) than does either of the soft-apertured profiles.

Combined with the exponential increase in scattering cross section with decreasing altitude the relatively slow decrease of the diffraction wings for the uniformly illuminated square $I \propto x^{-2}$ versus $I \propto x^{-4}$ for the truncated square-base pyramid prismoid and $I \propto \exp[-x^2]$ for the gaussian, where x is the distance from the beam axis in local beam width units) causes the part of the far-field pattern that is directly in the line of sight to the laser guide star for altitudes below about 30 km to dominate the Rayleigh scattering contribution to the image at and near the guide star angular position. This contribution cannot be eliminated by spatial filtering so it is imperative to keep hard truncation of the initial irradiance profile to a minimum at least in the transverse direction corresponding to the offset between the observing telescope and the laser beam director.

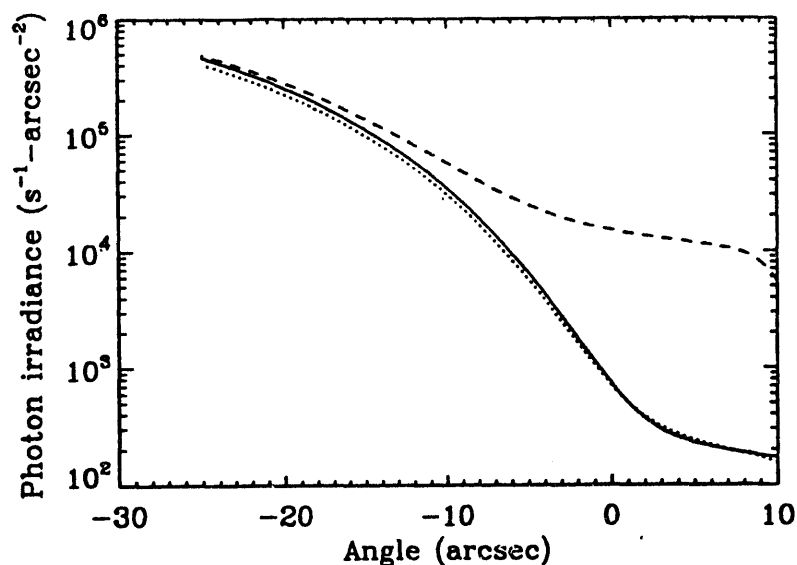


Figure 16. Comparison of calculated Rayleigh scattered light profiles along the projection of the laser beam axis onto the camera image plane for the following laser beam irradiance profiles at the beam director: a uniformly illuminated square (dashed line), a truncated square-based pyramid prismoid with a 2:1 ratio of base-to-top edge lengths (dotted line), and an untruncated gaussian (solid line). The 0.25 m diameter telescope is focused at infinity. Turbulence $r_0 = 5$ cm at 589 nm and an exponential air density profile with a scale height of 7.3 km are used. The numerical values are for 1 kW and no optical or atmospheric transmission losses.

In Figure 17 the experimentally measured image of Rayleigh backscatter (dashed line) is compared to the calculated one (dotted line) for the uniformly illuminated square aperture. The agreement is excellent considering that no aerosol scattering contribution is included in the calculation and that scattering from the Mt. Pinatubo volcanic aerosol layer was clearly visible to the naked eye during the experiment on August 27, 1992. The measurement represented by the dashed curve was obtained by detuning the laser 2.6 GHz and turning off the modulation to suppress emission from the mesospheric sodium layer. For comparison, the 589 nm backscatter image for an on-resonance modulated laser beam with the laser guide star centered at zero arcsec is also shown (solid line). The laser power was 658 W for both experimental curves and 0.61 was the measured atmospheric transmission coefficient. The calculated curve in Figure 17 is scaled to match the experimental power, the measured atmospheric transmission, and the 1976 U. S. Standard Atmosphere's density at 20 km altitude instead of at sea level. The result is between that of the on-resonant and off-resonant experimental values at an angle of -25 arcsec; the curve in Figure 17 is scaled by an additional factor of 1.07 to approximately match the on-resonant experimental value.

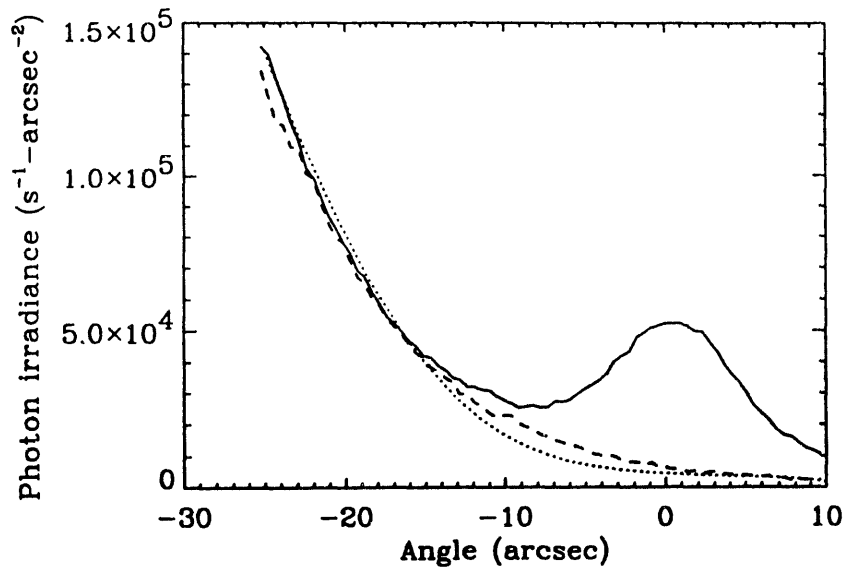


Figure 17. Comparison of calculated and observed (dashed line) Rayleigh scattered light profiles along the projection of the laser beam axis in the camera image plane. The experimental laser beam was 658 W of narrow bandwidth light detuned by 2.4 GHz from the sodium D_2 line center. For comparison the backscattered light profile with the laser on-resonance and modulated to broaden its spectrum to approximately match that of the D_2 line is also shown (solid line); the peak at zero arcsec is the signal from the sodium layer. The calculated curve is directly proportional to the dashed line curve in Figure 16.

4.5 Tip-Tilt system

The tip-tilt system described in section 3 was designed to operate in either the 1/2 m LLNL AO package or the AO package designed for use on the Lick Observatory 40 inch telescope. The results reported here were obtained on the 40 inch Lick telescope. Figure 18 shows the image of the binary star pair Alpha Gemini with no tip-tilt correction and with the tip-tilt control loop closed. The imaging wavelength was 1000 nm and the exposure time was 30 seconds. The graph at lower right are cuts through the two images showing the intensity profile for the two cases. The image improvement was about what was expected for tip-tilt only correction and the seeing conditions, for which D/r_0 was about 10. Here D is the telescope diameter and r_0 is the seeing cell size or the coherence length.

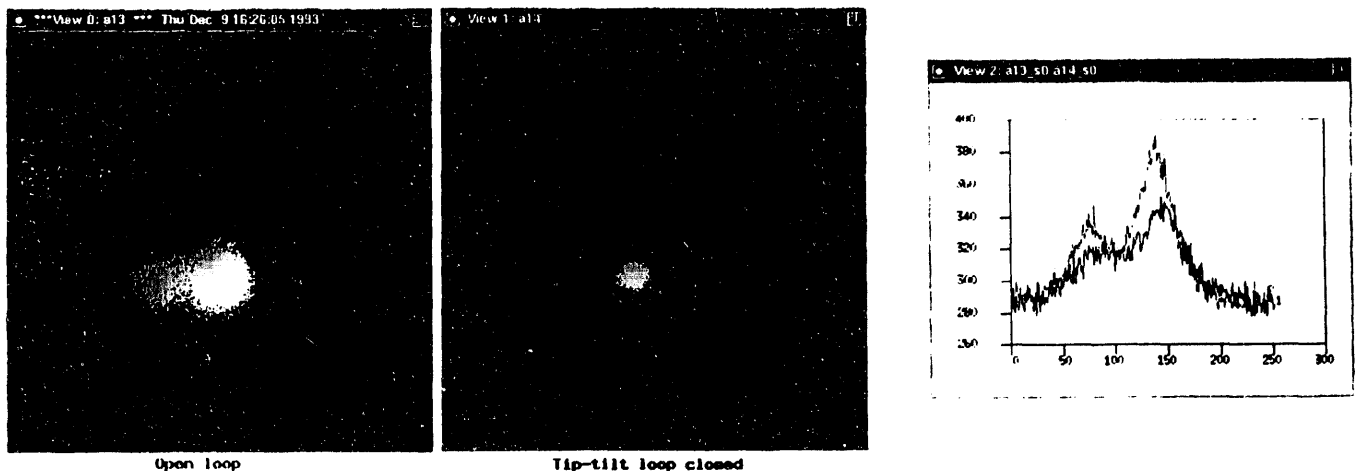


Figure 18. Binary star image at 1000 nm with the tip-tilt control loop open and closed. At right is the intensity profile of the two images.

The performance of the tip-tilt loop on another night (2/25/94), for which the seeing was better, are illustrated in Figures 19 and 20. The tilt power spectra while observing the star Pollux are shown in Figure 19. The top graph shows the x-axis open and closed loop spectra, and the bottom graph the y-axis data. The separation between the open and closed loop curves represents the disturbance rejection at that frequency. The disturbance rejection at 1 Hz is 54 dB and the gain crossover frequency is about 100 Hz.

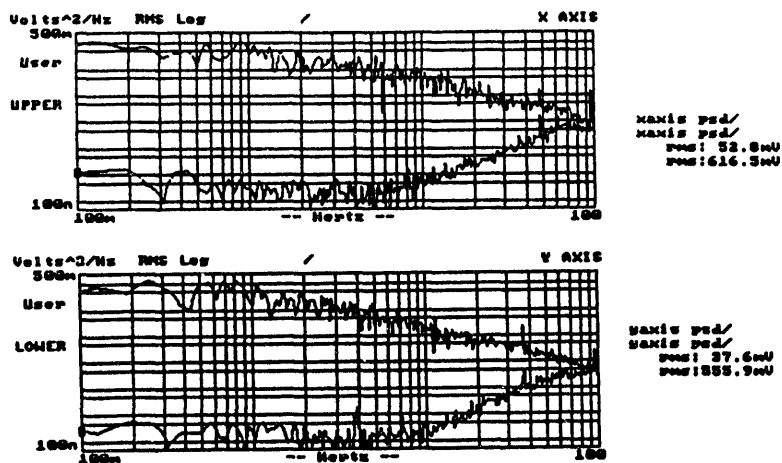


Figure 19. Tilt power spectrum in the x and y axis of the star Pollux with the tip-tilt loop open and closed.

The sensor was calibrated in arcsec/v so that the rms motion in arcsec could be determined. The rms 2-axis motion was found to be 0.42 arcsec open loop and 0.03 arcsec closed loop. The 2-axis rms motion, θ , is related to the seeing, S , which is the measured FWHM of a star image, by

$$S = [\theta / 0.6 * (\lambda / D)^{1/6}]^{6/5}; \text{ and } r_0 \text{ is given by } r_0 = \lambda / S.$$

For $\lambda = 900 \text{ nm}$, which is the peak response of the tip-tilt sensor, $D = 1 \text{ meter}$, and the measured $\theta = 0.42 \text{ arcsec}$, one obtains a seeing of 0.9 arcsec. The measured FWHM on the science camera was 1.0 arcsec. The r_0 derived from the tilt spectrum is then 21 cm at 900 nm which corresponds to an r_0 of 11.6 cm at 550 nm. Figure 20 shows a 3-D view of the star Arcturus with the tip-tilt loop open and closed. This was taken at a wavelength of 1000 nm, for which D/r_0 was about 5. The peak intensity increased by 50% and the image FWHM went from 1.0 to 0.6 arcsec.

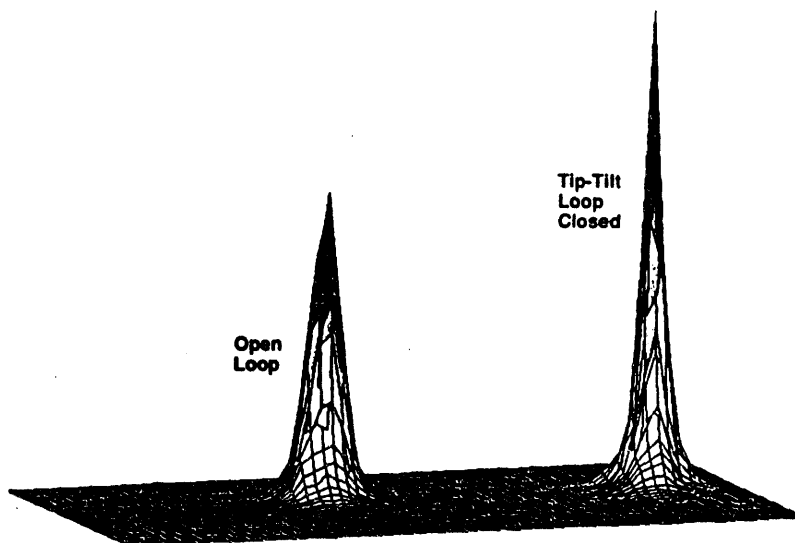


Figure 20. Three dimensional representation of the star Arcturus image with the tip-tilt loop open (left) and closed (right).

5. CONCLUSIONS AND FUTURE PLANS

The experimental program at LLNL, although it did not reach the goal of a full AO system operating on the 1/2 m telescope with a sodium laser guide, was successful in demonstrating its feasibility. An AO system is now operational on the Lick Observatory 40 inch telescope with natural stars, and will be placed on the Lick 120 inch Shane telescope and operating with a 20 watt laser by the end of 1994. In 1995 the astrophysical observation program will start with the system designed for operation at about 2 microns. This system uses a 69 actuator deformable mirror which will be replaced with a 127 actuator mirror permitting operation at wavelengths of 0.7 - 0.8 microns.

6. ACKNOWLEDGMENTS

This research was performed under the auspices of the U.S. Department of Energy, under contract number W-7405-ENG-48 to the Lawrence Livermore National Laboratory. The LLNL Laser Guide Star Project is supported by the LLNL Laboratory Directed Research and Development Program. Related work is supported by the Institute of Geophysics and Planetary Physics and by the Engineering Department at LLNL. We would like to thank the large group of LLNL technical staff who provided support in the operation of the AVLIS lasers and the guide star site operations.

7. REFERENCES

1. J.T. Salmon, K. Avicola, J.W. Bergum, S.D. Mostek, R.W. Presta, R.J. Rinnert, C.W. Swift, C.L. Weinzapfel, and J.N. Wong, "An adaptive optics package designed for astronomical use with a laser guide star tuned to an absorption line of sodium", to be published in Proc SPIE, 2201 (1994).
2. W. Happer, G. MacDonald, C. Max, and F. Dyson, "Atmospheric turbulence compensation using resonant backscattering from the sodium layer in the upper atmosphere" J. Opt. Soc. Am. A., 11, No.1, 263-276. (1994)
3. R. Foy and A. Labeyrie, "Feasibility of adaptive optics telescope with laser probe", Astronomy and Astrophysics, 152, L29-L31 (1985).
4. L.A. Thompson and C.S. Gardner, "Experiments on laser guide stars at Mauna Kea Observatory for adaptive imaging in astronomy", Nature, 328, 229-231 (1987).
5. R.A. Humphries, C. Primmerman, L. Bradley, and J. Hermann, "Atmospheric turbulence measurements using a synthetic beacon in the mesospheric sodium layer", Optics Letters, 16, 1367-1369 (1991).
6. R.Q. Fugate, B.L. Ellerbroek, C.H. Higgins, M.P. Jelonek, W.J. Lange, A.C. Slavin, W.J. Wild, J.M. Spinhirne, B.R. Boeke, R.E. Ruane, J.F. Moroney, M.D. Oliker, D.W. Swindle, and R.A. Cleis, "Two generations of laser-guide-star adaptive-optics experiments at the Starfire Optical Range", J. Opt. Soc. Am. A, 11, No. 1, 310-324, (1994).
7. R.P. Hackel, B.E. Warner, "The copper-pumped dye laser system at Lawrence Livermore National Laboratory", Proc SPIE, 1859, 120-129 (1993).
8. K. Avicola, J.M. Brase, J.R. Morris, H.D. Bissinger, J.M. Duff, H.W. Friedman, D.T. Gavel, C.E. Max, S.S. Olivier, R.W. Presta, D.A. Rapp, J.T. Salmon, and K.E. Waltjen, "Sodium-Layer Laser Guide Star Experimental Results", J. Opt. Soc. Am.A, 11, No. 2, 825-831, (1994).
9. S.S. Olivier, K. Avicola, H.D. Bissinger, J.M. Brase, W. Fisher, H.W. Friedman, D.T. Gavel, E.M. Johansson, B. Johnston, C.E. Max, D.A. Rapp, and K.E. Waltjen, "Performance of adaptive optics at Lick Observatory", to be published in Proc SPIE, 2201 (1994).
10. J.M. Brase, K. Avicola, H.D. Bissinger, W.A. Fisher, H.W. Friedman, D.T. Gavel, B. Johnston, C.E. Max, S.S. Olivier, D.A. Rapp, J.T. Salmon, K.E. Waltjen, "Adaptive optics at Lick Observatory: system architecture and operations", to be published in Proc SPIE, 2201 (1994).
11. H. Friedman, T. Kuklo, N. Wong, R. Page, and G. Thompson, "Design of a fieldable laser system for a sodium guide star", to be published in Proc SPIE, 2201 (1994).
12. K. Avicola, J.T. Salmon, J.M. Brase, K.E. Waltjen, R.W. Presta, and K.S. Balch, "High frame-rate, large field wavefront sensor", Laser Guide Star Adaptive Optics Workshop Proceedings, Vol. 2, (Phillips Laboratory, Albuquerque, N.M., March 1992).
13. C.E. Max, K. Avicola, J.M. Brase, H.W. Friedman, H.D. Bissinger, J. Duff, D.T. Gavel, J. A. Horton, J.R. Morris, S.S. Olivier, R.W. Presta, D.A. Rapp, J. T. Salmon, and K.E. Waltjen, "Design, layout, and early results of a feasibility experiment for sodium-layer laser guide star adaptive optics", J. Opt. Soc. Am.A, 11, No 2, 813-824, (1994).
14. J.R. Morris, "Efficient excitation of a mesospheric -sodium laser guide star by intermediate duration pulses", J. Opt. Soc. Am.A, 11, No.2, 832-845, (1994).
15. J. W. Goodman, Statistical Optics, (John Wiley, New York, 1985), pp. 402-407.

Doc I

**DATE
FILMED**

8/18/94

END

